Low-Energy Sputter Erosion of Various Materials in a T5 Ion Thruster*†

Jenny R. Gruber
University of Oxford‡
Department of Engineering Science
Osney Laboratory
Oxford OX1 3PJ
United Kingdom
+44-1865-288762
jennifer.gruber@univ.ox.ac.uk

IEPC-01-307

Samples of molybdenum, amorphous graphite, and Invar were mounted—one material at a time—inside a graphite QinetiQ T5 ion thruster discharge chamber and biased at different potentials with respect to the discharge plasma potential. Discharge plasma properties were measured with Langmuir probes. Biasing the samples attracted ions at known energies, ranging from 50-150 eV. By monitoring the ion current to each sample over the duration of the experiment and measuring the mass of the samples before and after ion bombardment, a quantitative calculation of sputter yield was made for each sample. Results for molybdenum and Invar matched Yamamura and Tawara's 1996 semi-empirical sputter formula. The amorphous graphite samples showed significant erosion due to sputtering when biased below the predicted threshold energy, suggesting that sputter threshold is still not fully understood. Erosion rates in mg/hour are also presented for each material and bias, with graphite having 1/30 to 1/10 the erosion rates of the other materials.

Introduction

In ion engines, thruster components experience erosion due to a process called ion sputtering. This erosion can be divided into two types: high-energy sputtering of the grids, and low-energy sputtering of the discharge chamber components. Grid erosion is generally recognised as the main lifetime-limiting mechanism for ion engines[1-3]. However, erosion of discharge chamber components does limit performance[1,4] and can potentially cause grid shorts due to spalling[5,6].

Discharge chamber erosion is also worthy of consideration because performance in the chamber affects grid erosion. If more propellant is ionised in the discharge chamber, fewer neutral particles leave the chamber, and there is less grid erosion due to charge-exchange ions. Charge exchange erosion is the dominant wear mechanism for the accelerator grid[7,8].

To ionise more propellant in the discharge chamber, the electron energy, and therefore the plasma potential, must be increased. Sputtering in the discharge chamber is related to the plasma potential, so an increase in plasma potential means an increase in erosion due to sputtering.

The ions in the discharge chamber of the Kaufmann ion thruster have energies well below 100 eV. No previous experimental sputter yield data have been reported for sputtering below 100 eV with xenon ions incident on materials commonly used in ion thrusters[9-11]. Increased knowledge of low-energy sputtering could lead to better lifetime predictions for discharge chamber components and greater understanding of trade-offs between maximised thruster performance and increased sputter erosion.

This paper describes research that was conducted to gather data on low-energy sputtering of a variety of materials through a range of energies. An ion thruster

* Presented as Paper IEPC-01-307 at the 27th International Electric Propulsion Conference, Pasadena, CA, 15-19 October, 2001.

‡ Experimental work conducted at QinetiQ, Farnborough, UK.

was used as an ion source, with material samples mounted in the discharge chamber and biased at different potentials to attract ions at a range of energies. The ion current to each material sample was monitored over the duration of the experiment, and the mass of the samples was measured before and after ion bombardment. Knowing the ion current and mass loss, quantitative calculations of sputter yield—defined as the number of atoms sputtered for each incident ion—were made for each sample. Attempts were made to account for doubly charged ions.

Sputter Yield

Empirical Formula

In 1969, Sigmund published the following formula for sputter yield with normally incident ions onto a monatomic surface based on the Boltzmann transport equation[12]:

$$Y = \frac{0.042\alpha S_n}{U_s} \tag{1}$$

Y is sputter yield, S_n is the nuclear stopping cross-section, and α is a function of the masses of the incident ion and the target atom. U_s is the surface binding energy of the target material and is generally assumed to have the same value as the heat of sublimation. This formula works well for most sputter scenarios, but is not accurate for sputtering by light or low-energy incident ions[9].

The semi-empirical sputter yield formula evolved, changing often as new data were gathered. The latest, most comprehensive semi-empirical equation was published by Yamamura and Tawara in 1996[9]:

$$Y = \frac{0.042Q\alpha^*}{U_s}\frac{S_n}{1+\Gamma k_e \varepsilon^{0.3}}\left[1-\left(E_{th}/E\right)^{1/2}\right]^s \tag{2}$$

Q and s are fitting parameters, dependent on the target material. Yamamura and Tawara provide a table of these parameters for an extensive list of elements. E is the energy of the incident ion, and E_{th} is the threshold energy. The threshold energy is the energy of the incident ion below which sputtering should not occur. The other components of the equation are defined as follows:

$$\alpha^* = \begin{cases} 0.249\left(\frac{M_2}{M_1}\right)^{0.56} + 0.0035\left(\frac{M_2}{M_1}\right)^{1.5} & M_1 \le M_2 \\ 0.0875\left(\frac{M_2}{M_1}\right)^{-0.15} + 0.165\left(\frac{M_2}{M_1}\right) & M_1 \ge M_2 \end{cases} \tag{3}$$

M_1 and M_2 are the masses of the incident ion and target atoms, respectively.

$$S_n = \frac{84.78 Z_1 Z_2}{\left(Z_1^{2/3}+Z_2^{2/3}\right)^{1/2}}\frac{M_1}{\left(M_1+M_2\right)}s_n \tag{4}$$

Z_1 and Z_2 are the atomic numbers for the incident ion and the target atom elements, and s_n is the reduced nuclear stopping power:

$$s_n = \frac{3.441\sqrt{\varepsilon}\ln\left(\varepsilon+2.718\right)}{1+6.35\sqrt{\varepsilon}+\varepsilon\left(6.882\sqrt{\varepsilon}-1.708\right)} \tag{5}$$

The reduced energy, ε, is:

$$\varepsilon = \frac{M_2}{\left(M_1+M_2\right)}\frac{0.03255}{Z_1 Z_2\left(Z_1^{2/3}+Z_2^{2/3}\right)^{1/2}}E \tag{6}$$

Γ is a parameter describing the contribution to sputter yield of the mechanism whereby ions penetrate deep into the surface of the material, collide with atoms, and are reflected back to sputter material at the surface. This mechanism is most common with light, fast incident ions. The other mechanism accounted for in this semi-empirical equation is most common with slow, heavy ions and consists of the ion interacting with and causing cascades amongst the atoms near the surface of the material.

$$\Gamma = \frac{W}{1+\left(M_1/7\right)^3} \tag{7}$$

W is another fitting parameter that is dependent on target material and given in a table in reference 9. k_e is the Lindhard electronic stopping coefficient:

$$k_e = 0.079\frac{\left(M_1+M_2\right)^{3/2}}{M_1^{3/2}M_2^{1/2}}\frac{Z_1^{2/3}Z_2^{1/2}}{\left(Z_1^{2/3}+Z_2^{2/3}\right)^{3/4}} \tag{8}$$

Yamamura and Tawara define the threshold energy as:

$$E_{th} = \begin{cases} \dfrac{\left[1 + 5.7\left(M_1 / M_2\right)\right] U_s}{\gamma} & M_1 \le M_2 \\ 6.7 U_s / \gamma & M_1 \ge M_2 \end{cases} \quad (9)$$

γ is the energy transfer factor, representing the maximum energy transferred in an elastic collision:

$$\gamma = \frac{4 M_1 M_2}{\left(M_1 + M_2\right)^2} \quad (10)$$

In this experiment, the ions are believed to be normally incident onto the surfaces of the material samples because the mean free path between ion collisions with other ions and neutral atoms is much larger than the sheath thickness.

Although Invar is not a monatomic solid, the above equations are valid for calculating Invar sputter yields. For iron- and nickel-based alloys—Invar is a 36% nickel-iron alloy—the calculated sputter yield is assumed to be a weighted combination of the contributions to sputter yield of each element[13].

Threshold Energy

The value and even the existence of threshold energy for every ion-target combination have been widely debated. A variety of equations—mainly based on binding energy, the energy transfer factor, and some experimental data—have been published for threshold energy for ions with both normal and oblique incidences[9,14-17].

For most materials used in this experiment, the threshold energy for bombardment with xenon atoms is assumed to be lower than 50 eV. The energies studied in this experiment were between 50 and 150 eV, so the threshold limit was not explored for these materials. The exception was carbon, which in most literature is assumed to have a threshold higher than 130 eV when bombarded by normally incident xenon ions[9,15].

Experiment

The ion source is a QinetiQ T5[1] discharge chamber—the apparatus is shown in Figure 1. The anode and chamber wall are made of amorphous graphite, and the backplate, inner pole, outer pole, and baffle are shielded with amorphous graphite. A graphite T5 was chosen because graphite is believed to have a much lower sputter yield than materials normally used. During the experiment, sputter from discharge chamber components could deposit on the material samples, causing error in the sputter yield measurements. Using a material with a low sputter yield minimises the error due to sputter deposits from the discharge chamber components.

Because the thruster was only used as an ion source and no beam was drawn, there was no neutraliser and a single, 5-mm thick carbon grid replaced the triple-grid acceleration system. This grid was used to mount the material samples and to maintain the gas pressure within the discharge chamber at a nominal level.

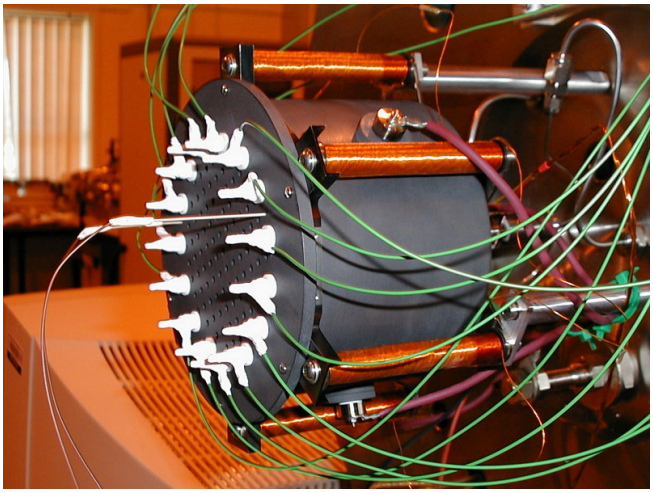

Figure 1—Graphite T5 with modified mounting grid, material samples, and Langmuir probes

The thruster settings were different from those of nominal operations. For each experiment, parameters were adjusted until the discharge voltage was near 40 V and as steady as possible. Because no beam was drawn, no main flow was necessary to ensure adequate current to the material samples. For comparison, Table 1 lists nominal operating parameters for the T5, as well as operating parameters for this experiment.

Table 1. Comparison of Thruster Parameters for Nominal Operations and Erosion Experiment

	Nominal	Erosion Experiment
Discharge Voltage	38 V	34.6-43.0 V
Discharge Current	2.6 A	1.3-1.5 A
Magnet Current	200 mA	300-400 mA
Cathode Flow Rate	0.1 mg/s	0.1 mg/s
Main Flow Rate	0.6 mg/s	None

In each experiment, 15 material samples—all made of the same material—were mounted on the grid at a radius of 4.5 cm. Each of the samples was biased at a different potential with respect to the anode. The difference between the anode and plasma potentials was determined using Langmuir probes periodically throughout the duration of each experiment. For graphite, the sample biases ranged from 50-150 V, and for the other materials the biases ranged from 50-100 V.

Two cylindrical Langmuir probes were mounted on the grid (see Figure 1) at the same radius as the material samples and with their tips approximately 3.5 mm closer to the backplate than the sample surfaces. One was made of molybdenum and the other of tantalum, and both had a tip of length 2 mm and radius 0.5 mm. Molybdenum and tantalum have different work functions, so both probes were used for each measurement in order to account for errors due to photoemission or secondary electron emission. Contamination is usually not a problem for xenon plasmas in cryopumped vacuum systems[18], but as a precaution, the probes were subjected to ion bombardment to clean them before taking each trace.

Prior to each experiment, the material samples were weighed using a microbalance with a sensitivity of 0.1 μg at the National Physical Laboratory in Teddington, UK. The samples were weighed again after ion bombardment to determine their mass loss.

The bias of each material sample with respect to the anode potential and the ion current to each material sample were monitored throughout each experiment using a data acquisition unit. The ion current density ranged from 1.9-4.8 mA/cm^2. The mass loss and ion current were used to calculate sputter yield. The biases of the samples with respect to anode potential, along with Langmuir probe data on plasma potential, were used to calculate the ion energies to within ±1V.

During each experiment, one of the mounted samples was biased at a low potential (6 V or lower). This sample did not sputter and instead collected deposits from the sputtering of the other samples and discharge chamber components. The amount of deposit on this sample was used to estimate error in the sputter yield measurements due to sputter deposition.

For each experiment, several extra material samples were made and weighed. These extra samples were then subjected to everything that the experimental samples were subjected to, except for sputtering. The changes in mass of the extra samples were used to calculate error from material loss in the samples due to non-sputter processes like outgassing in vacuum and any drift in the microbalance.

The thruster was mounted in a 0.5-m diameter vacuum chamber, cryopumped to a background pressure of approximately 5 x 10^{-8} torr with the thruster off. The background pressure stayed just under 10^{-5} torr with the thruster on. Partial pressures of certain gases were measured throughout each experiment, using a mass spectrometer mounted on the vacuum chamber. When the thruster was running, partial pressures of water and air were on the order of 10^{-9} torr, and O_2 and carbon dioxide were on the order of 10^{-10} torr.

A high facility background pressure can affect sputter yield. In particular, nitrogen chemisorbs to molybdenum, creating a buffer and causing the measured sputter yield to be lower than it would be in a completely clean environment[19]. Also, oxygen, water vapour, and nitrogen have been shown to react with carbon, causing it to erode more and appear to have a higher sputter yield than it should[20]. In this experiment, the facility background pressure and partial pressures were low enough to assume that they would have little affect on sputter yield.

Each experiment tested a different material and lasted approximately 200 hours.

Results and Discussion

Erosion Rates

Erosion rates are given for each material and bias in Figure 2. Over the range of 50-100 eV, the erosion rates for molybdenum and Invar are comparable and are 10-30 times greater than those for amorphous

graphite. Also, the increase in erosion rates for graphite is shallower than for the other materials. Over the range of 50-100 eV, the erosion rate for graphite increases approximately one order of magnitude. Over the same range, the erosion rates for the other materials increase by nearly two orders of magnitude. This suggests that a large increase in discharge plasma potential would have a much smaller impact on erosion of graphite discharge chamber components than on erosion of components made of molybdenum or Invar.

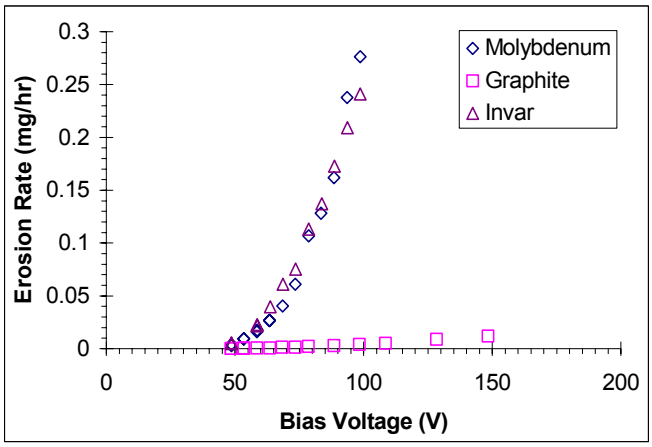

Figure 2—Comparison of Erosion Rates for Different Materials

Sputter Yields

For each material sample, the mass loss in atoms is found by dividing the mass loss in mg by atomic weight of the sample material. The total number of ions that struck the surface of a material sample is found by multiplying the current to that sample by the duration of the experiment and dividing by 1.6×10^{-19} C.

If all of the ions in the discharge plasma were singly charged, the sputter yield calculation would simply consist of dividing mass loss in atoms by the total number of ions that struck the surface of the material. However, there is most likely some small quantity of doubly charged particles in the discharge plasma. For the QinetiQ T5 operating with an anode voltage in the range of those seen in this experiment, the ratio of doubly to singly charged ions is between 2 and 10%, and the presence of triply charged ions is so small it can be neglected[21].

In reference 21, data were gathered showing that the fraction of doubly charged particles is dependent on anode voltage and main flow rate. As anode voltage increases, so does the fraction of doubly charged particles. This fraction also increases as flow rate is decreased, implying that for this experiment there should be a high fraction of doubles. However, the sputter yield data suggest that this fraction is low. For comparison, attempts were made to account for doubles based on doubly charged ion fractions of 1%, 5%, and 10%.

Doubly charged particles change the calculation of the total number of ions to the surface because they contribute twice the charge of a singly charged ion to the ion current. Also, for a material sample set at a particular bias, doubly charged ions will bombard the surface of the sample with twice the energy of singly charged ions, and will therefore cause a larger amount of sputtering and influence the sputter yield calculation. These factors are considered when attempting to account for doubly charged ions in the sputter yield calculation.

Assuming Only Singly Charged Particles

Sputter yields are given for each material and ion energy in Figure 3. These yields were calculated assuming no doubly charged ions bombarded the material samples. The sputter yields for molybdenum and Invar are comparable and noticeably higher than the sputter yields for amorphous graphite. The sputter yields for graphite increase more slowly than those for the other materials as energy increases. These results are not surprising, considering the erosion rates shown in Figure 2.

One thing to note is that the difference between molybdenum erosion and Invar erosion is much more pronounced in Figure 3 than in Figure 2—although the two are still comparable. There are two reasons for this. First, the atomic mass of Invar is slightly lower than that of molybdenum, so a comparable loss in mg would give a higher atomic loss for Invar. Also, the ion current densities to the material samples were slightly lower in the Invar experiment than in the molybdenum one, so fewer ions bombarded the Invar samples.

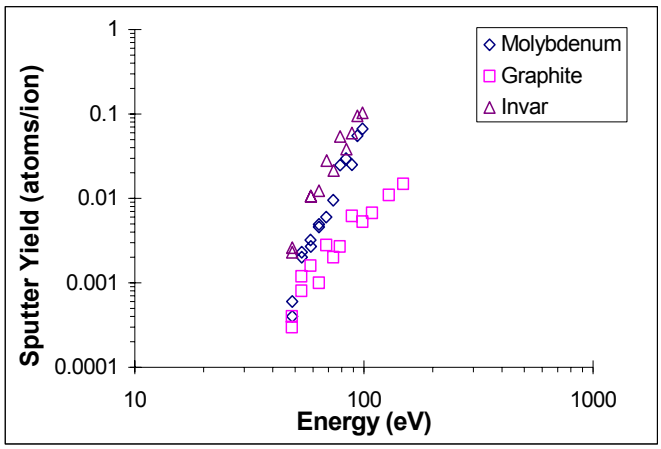

Figure 3—Comparison of Sputter Yields for Different Materials, Assuming No Doubly Charged Ions

The methods used to account for doubly charged ions are not applicable—for reasons given in the next section—to sputtering by xenon ions on graphite at the energies seen in this experiment. Therefore, the experimental sputter yields for amorphous graphite can only be calculated assuming no doubles. These sputter yields are shown in Figure 4, along with the sputter yield curve for xenon incident on carbon, calculated using equation (2).

These data suggest that threshold predictions for carbon are still inaccurate. Most published equations predict a threshold higher than 130 eV for xenon ions incident on carbon[9,15], meaning that for this experiment, no samples biased at less than 65 V should have seen any sputtering—not even by doubly charged ions. All of the samples in this experiment experienced noticeable erosion, even those biased at 50 eV. The inaccuracy of the threshold prediction may account for the experimental data being shifted so far from the equation (2) curve.

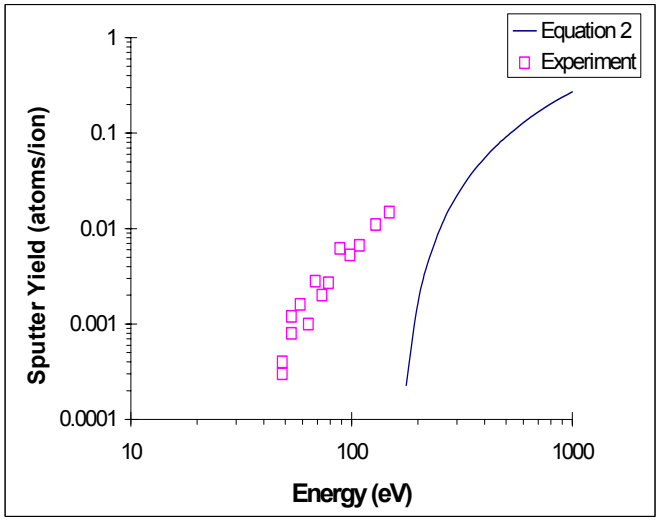

Figure 4—Comparison of Experimental Sputter Yield Data with Curve from Equation (2) for Amorphous Graphite, Assuming No Doubly Charged Ions

Accounting for Doubly Charged Particles

Two methods are used to attempt to account for doubly charged particles. Method 1 assumes that equation (2) can accurately predict sputter yields for incident ions with the energies of the doubly charged particles. This is a reasonable assumption because past experimental work done for ions at 100 eV and above has agreed fairly well with the Yamamura and Tawara equation[9].

For each sample, equation (2) is used to determine sputter yield for ions bombarding the target material with energy equal to double the sample's bias. A doubly charged ion fraction of 1, 5, or 10% is assumed. The mass loss of the sample due to doubly charged ions is then determined by multiplying sputter yield by the total number of doubly charged ions that struck the sample surface. This mass loss is then subtracted from the total mass loss of the sample. The remaining mass loss is due to singly charged ions and is divided by the total number of singly charged bombarding ions to determine experimental sputter yield for xenon ions bombarding the target material with energy equal to the sample's bias.

This method is not applicable for the amorphous graphite because equation (2) predicts a threshold energy of 160.8 eV for xenon incident on carbon. The amorphous graphite samples were biased at potentials between 50 and 150 eV. Thus, for the majority of the graphite samples, equation (2) could not be used to predict a sputter yield for doubly charged ions, and this method is invalid.

Method 2 assumes that equation (2) accurately predicts the ratio between sputter yield for ions with the energy of the doubly charged particles and sputter yield for ions with the energy of the singly charged particles. For each sample, this ratio, the singly charged ion current, and the doubly charged ion current are used to calculate the contributions to the total mass loss of the singles and of the doubles. These contributions to mass loss can then be divided by their respective ion currents to determine experimental sputter yields, both

for ions bombarding the target material with energy equal to the sample's bias, and for ions bombarding the target material with energy equal to twice the sample's bias.

This method is not applicable for the amorphous graphite because it uses predictions of sputter yield by equation (2) for ions with energies equal to the material sample biases as well as for ions with energies equal to double the material sample biases. For the range of biases to the graphite samples, equation (2) cannot predict sputter yields for xenon ions incident on carbon with energies equal to the sample biases, so this method is invalid.

Figures 5a and 5b give sputter yields calculated using Method 1 and Method 2, respectively, for the molybdenum samples. For comparison, both figures show the equation (2) curve for xenon ions incident on molybdenum, as well as sputter yields calculated from experimental data, assuming doubly charged ion fractions of 1, 5, and 10% of the total number of ions.

For both Method 1 and Method 2, the sputter yields calculated from experimental data have good agreement with sputter yields predicted by equation (2), and there is little difference in the calculated values for the different fractions of doubly charged ions. The calculated sputter yields appear to be little influenced by doubly charged ion fractions for values below 10%.

The exception is that, for Method 1, there are fewer values of sputter yield calculated from experimental data when the fraction is assumed to be 5% or 10%. At the lower energies, if the doubly charged ions produce sputter yields as predicted by equation (2), and if they constitute 5 or 10% of the total number of ions, the contribution to mass loss of the doubly charged ions is actually larger than the total measured mass loss. This would suggest that the fraction of doubly charged ions is lower than 5%.

This would also explain the much lower Method 2 calculated sputter yields for 5 and 10% at 50 and 100 eV, shown in Figure 5b.

Figures 6a and 6b give sputter yields calculated using Method 1 and Method 2, respectively, for the Invar samples. Again, for both methods, the sputter yields calculated from experimental data have good agreement with sputter yields predicted by equation (2), although the experimental sputter yields are a bit lower. There is, again, little difference in the calculated values for the different fractions of doubly charged ions. These data also suggest that the fraction of doubly charged ions is less than 5% of the total number of ions. Indeed, the best fit with the semi-empirical formula is obtained if it is assumed that there are no doubly charged ions in the discharge.

Conclusions

These discharge chamber erosion experiments have shown that, for molybdenum and Invar, the Yamamura and Tawara semi-empirical sputter equation can be used to predict erosion rates with reasonable accuracy for materials bombarded by ions with energies down to 50 eV. It is likely that the erosion of any material for which this equation gives a sputter threshold of less than 50 eV can also be predicted this way.

The erosion of the graphite samples at energies well below the predicted threshold for carbon suggests that threshold equations—and even the existence of a true threshold value—need to be reconsidered. Although graphite did sputter more than expected at low energies, it still had much lower erosion rates than the other materials, suggesting that it is the best material for discharge chamber components if erosion is the main concern. The shallow increase of the graphite erosion rate as ion energy increases suggests that graphite is also a good option when flexibility in the discharge chamber's operating parameters is needed. This flexibility is crucial for throttling, high thrust density,

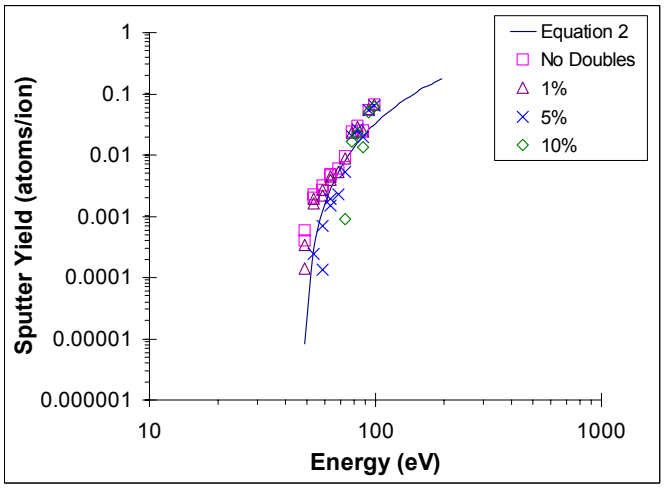

Figure 5a—Comparison of Experimental Sputter Yield Data Calculated Using Method 1 Assuming Doubly Charged Ion Fractions of 0, 1%, 5%, and 10% and Curve from Equation (2)—Molybdenum

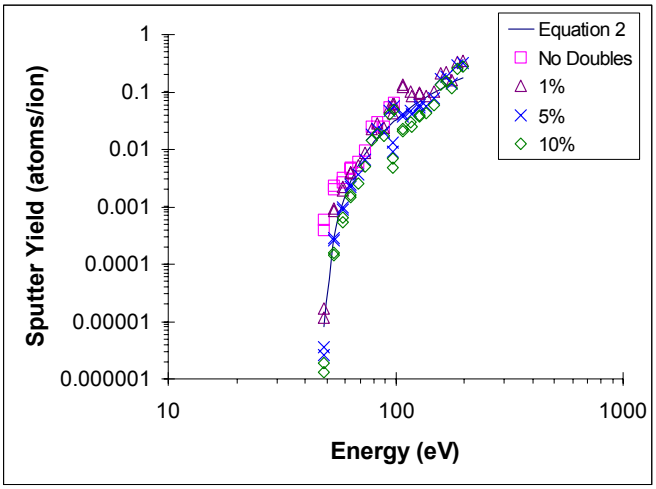

Figure 5b—Comparison of Experimental Sputter Yield Data Calculated Using Method 2 Assuming Doubly Charged Ion Fractions of 0, 1%, 5%, and 10% and Curve from Equation (2)—Molybdenum

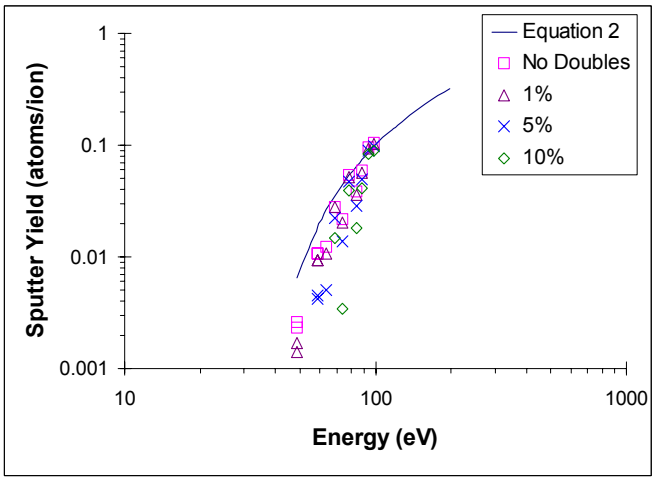

Figure 6a—Comparison of Experimental Sputter Yield Data Calculated Using Method 1 Assuming Doubly Charged Ion Fractions of 0, 1%, 5%, and 10% and Curve from Equation (2)—Invar

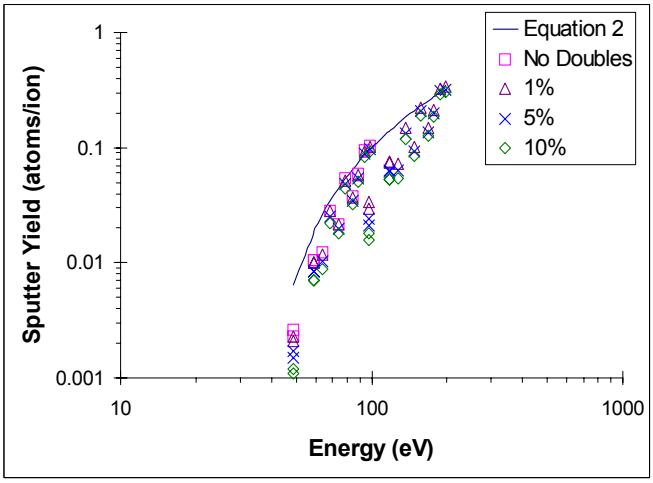

Figure 6b—Comparison of Experimental Sputter Yield Data Calculated Using Method 2 Assuming Doubly Charged Ion Fractions of 0, 1%, 5%, and 10% and Curve from Equation (2)—Invar

and increased mass utilisation efficiency. A small increase in mass utilisation efficiency can significantly increase grid lifetime.

The operating parameters for the discharge chamber used in this experiment were very different from the nominal parameters. No beam was drawn, there was no main flow, and because the material samples were biased to draw ions to a concentrated area, the current densities to the samples were much higher than the current densities to discharge chamber components during nominal operations. Therefore, the erosion rates measured in this experiment in units of mass loss per hour cannot directly be used to accurately predict

erosion of discharge chamber components in a thruster operating with nominal parameters. However, because each material was tested in similar conditions, the erosion rates found in this experiment can be used to make comparisons between the different materials.

Sputter yield data for tantalum, pyrolytic graphite, and Swedish iron will soon be found using the methods outlined in this paper. Other suggested future work includes experiments with ions near threshold energy and experiments with low energy ions at oblique incidences.

Acknowledgements

The author would like to thank Professors Terry Jones and John Allen of Oxford University, Neil Wallace of QinetiQ, Farnborough, and the members of the Electric Propulsion Group at QinetiQ, Farnborough for their advice and encouragement; Mike Kelly of QinetiQ, Farnborough and Dominic Harris of Oxford University for the excellent machining; Ian Severn and Stuart Davidson of the National Physical Laboratory in Teddington for the use of their microbalance; and the British National Space Centre, the Rhodes Trust, Oxford University's Department of Engineering Science, and University College, Oxford for their financial support.

References

[1] D. G. Fearn, "Ion Thruster Lifetime Limitations Imposed by Sputtering Processes," IEPC-93-177, September 13-16, 1993.

[2] V. Shutthanandan, P. K. Ray, N. R. Shivaparan, R. J. Smith, S. Thevuthasan, and M. A. Mantenieks, "On the Measurement of Low-Energy Sputtering Using Rutherford Backscattering Spectrometry," IEPC-97-069, August 24-28, 1997.

[3] C. J. Gaeta, J. N. Matossian, R. S. Turley, J. R. Beattie, J. D. Williams, and W. S. Williamson, "Erosion Rate Diagnostics in Ion Thrusters Using Laser-Induced Fluorescence," *Journal of Propulsion and Power* ***9*** *(3), 369-376,* May-June 1993.

[4] V. K. Rawlin, "Internal Erosion Rates of a 10-kW Xenon Ion Thruster," AIAA-88-2912, July 1988.

[5] M. W. Crofton, "Evaluation of the United Kingdom Ion Thruster," *Journal of Spacecraft and Rockets* ***33*** *(5), 739-747,* September-October 1996.

[6] J. L. Power and D. J. Hiznay, "Solutions for Discharge Chamber Sputtering and Anode Deposit Spalling in Small Mercury Ion Thrusters," AIAA-75-399, March 1975.

[7] J. M. Monheiser and P. J. Wilbur, "An Experimental Study of Impingement-Ion-Production Mechanisms," AIAA-92-3826, 1992.

[8] X. Peng, W. M. Ruyten, and D. Keefer, "Three-Dimensional Particle Simulation of Grid Erosion in Ion Thrusters," IEPC-91-119, 1991.

[9] Y. Yamamura and H. Tawara, "Energy Dependence of Ion-Induced Sputtering Yields from Monatomic Solids at Normal Incidence," *Atomic Data And Nuclear Data Tables* ***62*** *(2), 149-253,* March 1996.

[10] O. B. Duchemin, J. R. Brophy, C. E. Garner, P. K. Ray, V., Shutthanandan, M. A. Mantenieks, "A Review of Low Energy Sputtering Theory and Experiments," IEPC-97-068. 1997.

[11] W. Eckstein, C. Garcia-Rosales, J. Roth, and W. Ottenberger, "Sputtering Data," IPP 9/82 Max-Planck-Institut fur Plasmaphysik, Garching, February 1993.

[12] P. Sigmund, "Theory of Sputtering. I. Sputtering Yield of Amorphous and Polycrystalline Targets," *Physical Review* ***184*** *(2), 383-415,* August 10, 1969.

[13] J. Bohdansky, "Important Sputtering Yield Data for Tokamaks: A Comparison of Measurements and Estimates," *Journal of Nuclear Materials* ***93 & 94,*** *44-60,* 1980.

[14] M. A. Mantenieks, "Sputtering Threshold Energies of Heavy Ions," IEPC-97-187, August 24-28, 1997.

[15] W. Eckstein, C. Garcia-Rosales, and J. Roth, "Threshold Energy for Sputtering and Its Dependence on Angle of Incidence," *Nuclear Instruments and Methods in Physics Research B* ***83,*** *95-109,* 1993.

[16] E. Hotson, "Threshold Energies for Sputtering," *Nuclear Fusion* ***15,*** *544-547,* 1975.

[17] R. V. Stuart and G. K. Wehner, "Sputtering Yields at Very Low Bombarding Ion Energies," *Journal of Applied Physics* ***33*** *(7), 2345-2352,* July 1962.

[18] M. P. Monterde, M. G. Haines, A. E. Dangor, A. K. Malik, and D. G. Fearn, "Kaufman-Type Xenon Ion Thruster Coupling Plasma: Langmuir Probe Measurements," *Journal of Physics D: Applied Physics* ***30,*** *842-855,* 1997.

[19] M. A. Mantenieks and V. K. Rawlin, "Sputtering in Mercury Ion Thrusters," *NASA Technical Memorandum 79266,* 1979.

[20] J. S. Meserole, "Erosion Resistance of Carbon-Carbon Ion Optics," *Journal of Propulsion and Power* ***17*** *(1), 12-18,* January-February 2001.

[21] J. E. Pollard, "Plume Angular, Energy, and Mass Spectral Measurements with the T5 Ion Engine," AIAA-95-2920, July 1995.